Geochemistry Geophysics Geosystems G3
AN ELECTRONIC JOURNAL OF THE EARTH SCIENCES
Published by AGU and the Geochemical Society

Article
Volume 9, Number 6
14 June 2008
Q06O08, doi:10.1029/2007GC001760
ISSN: 1525-2027

Origin of the sheeted dike complex at superfast spread East Pacific Rise revealed by deep ocean crust drilling at Ocean Drilling Program Hole 1256D

Susumu Umino
Department of Earth Sciences, Kanazawa University, Kakuma-Machi, Kanazawa-Shi, Ishikawa 920-1192, Japan (sesumin@staff.kanazawa-u.ac.jp)

Laura Crispini
Dipartimento per lo Studio del Territorio e delle sue Risorse, Università di Genova, Corso Europa 26, I-16132, Genova, Italy (crispini@dipteris.unige.it)

Paola Tartarotti
Dipartimento di Scienze della Terra "A. Desio," Università degli Studi di Milano, via Mangiagalli, 34-20133, Milan, Italy (paola.tartarotti@unimi.it)

Damon A. H. Teagle
School of Ocean and Earth Sciences, Southampton Oceanographic Center, University of Southampton, European Way, Southampton SO14 3ZH, UK (dat@noc.soton.ac.uk)

Jeffery C. Alt
Department of Geological Sciences, University of Michigan, 2534 C.C. Little Building, Ann Arbor, Michigan 48109-1005, USA (jalt@umich.edu)

Sumio Miyashita
Department of Geology, Niigata University, Ninomachi 8050, Igarashi, Nishi-Ku, Niigata 950-2102, Japan (miyashit@geo.sn.niigata-u.ac.jp)

Neil R. Banerjee
Laboratory for Stable Isotope Science, Department of Earth Sciences, University of Western Ontario, Biology and Geological Sciences Building, London, Ontario N6A 5B7, Canada (neil.banerjee@uwo.ca)

[1] Superfast spread (22 cm/a) upper oceanic crust drilled at Ocean Drilling Program site 1256 comprises a thick sequence of extrusive lavas underlain by a thin region of sheeted dikes. The sheeted dikes at this site are characterized by the intimate association of in situ hyaloclastic fragmentation and hydrothermal alteration. Lithostatic and magmastatic pressure estimates reveal that there is no effective level of neutral buoyancy within the extrusive layer to trap dikes in the crust. This results in a situation that favors the extrusion rather than intrusion of magma. Fractures created by magmas rising in dikes were the loci of intense hydrothermal circulation and provided the pathways for subsequent dike intrusions. Magma-rich conditions expected for fast spreading ridge segments give rise to a rapid increase in magmatic pressure, which can result in dike intrusion even under only small deviatoric stress. This allows for the emplacement of narrow dikes in the upper crust, with magmas more likely to extrude, and hence the high extrusive/intrusive ratio for Site 1256.

Components: 10,142 words, 9 figures, 1 table.

Keywords: IODP; ODP Hole 1256D; sheeted dike complex; superfast spread mid-ocean ridge; East Pacific Rise; upper oceanic crust.

Index Terms: 3036 Marine Geology and Geophysics: Ocean drilling; 3035 Marine Geology and Geophysics: Midocean ridge processes; 8416 Volcanology: Mid-oceanic ridge processes (1032, 3614).

Received 17 July 2007; **Revised** 29 April 2008; **Accepted** 5 May 2008; **Published** 14 June 2008.

Umino, S., L. Crispini, P. Tartarotti, D. A. H. Teagle, J. C. Alt, S. Miyashita, and N. R. Banerjee (2008), Origin of the sheeted dike complex at superfast spread East Pacific Rise revealed by deep ocean crust drilling at Ocean Drilling Program Hole 1256D, *Geochem. Geophys. Geosyst.*, *9*, Q06O08, doi:10.1029/2007GC001760.

Theme: Formation and Evolution of Oceanic Crust Formed at Fast Spreading Rates

1. Introduction

[2] A sheeted dike complex is a distinctive constituent of most ophiolites and the key evidence for the formation of ocean crust in an extensional stress field [e.g., *Church and Stevens*, 1971; *Gass et al.*, 1981; *Glennie et al.*, 1974; *Kidd and Cann*, 1974; *Moores and Vine*, 1971; *Sturt and Thon*, 1978]. Sheeted dikes are the remnants of conduits that transferred magma from the magma chamber to the seafloor to be extruded as lava flows and the dikes accommodate the mid-crustal extension at spreading axes. The ophiolite lithostratigraphy as an analog of the uppermost oceanic crust has been confirmed by the drilling in Deep Sea Drilling Project (DSDP)/Ocean Drilling Program (ODP) Hole 504B in 6.9-Ma old oceanic crust formed at the Cocos-Nazca Spreading Center [*Alt et al.*, 1993; *Anderson et al.*, 1985; *Becker et al.*, 1988; *Dick et al.*, 1992] where 780.5-m thick extrusive rocks are underlain by >1056 m of sheeted dikes. In situ observations of sheeted dikes are also reported from exposures along escarpments bounding the Hess Deep Rift, which was formed at the fast spreading (135 mm/a) East Pacific Rise (EPR) [*Francheteau et al.*, 1992; *Hurst et al.*, 1994; *Karson*, 2002; *Karson et al.*, 1992]. At Hess Deep, although the thicknesses of the lavas and sheeted dikes vary considerably, the sheeted dikes (300–1200 m in thickness) are generally thicker than the extrusive lavas (150–700 m). Although only a limited number of direct observations of the entire upper oceanic crust are available, those studies suggest that the sheeted dike complex comprises a significant portion of the modern oceanic crust.

[3] *Ryan* [1994] proposed that sheeted dike complexes and the melt lenses on top of Axial Magma Chambers (AMCs) of mid-ocean ridges were formed by preferential emplacement of magmas at the Level of Neutral Buoyancy (LNB), where overall density of magma is equal to that of the country rocks, and magma is in local mechanical (gravitational) equilibrium with its surroundings. However, the AMC reflector depth ranges from 760 to 1550 m below the seafloor along the southern EPR between 13.8°S and 20.2°S, while density estimates based on the compressional wave velocity structures indicate the LNB depth of 200–700 m below the seafloor, which lies in the depth range from lower seismic layer 2A to layer 2B [*Hooft et al.*, 1997]. *Rubin* [1990] demonstrated that interaction of tectonic stress relaxation and magma supply results in higher ratios of intrusive to extrusive rocks and explains the common occurrence of wider dikes in Iceland than in Hawaii. The stress field in the lithosphere controls the driving force and frequency of dike intrusions [*Gudmundsson*, 1988, 1990] and modifies the LNB which determines the preferential site for dike emplacement [*Rubin*, 1995; *Takada*, 1989]. This Apparent Level of Neutral Buoyancy (apparent LNB) tends to lie at the brittle-ductile boundary [*Rubin*, 1990, 1995; *Watanabe et al.*, 1999]. Because hydrothermal circulation in the upper crust is vigorous and axial magma chambers at fast spreading ridge axes are underlain by wide regions of crystal mush, the brittle-ductile boundary is expected to occur between the base of the sheeted dikes and the roof zone of the axial magma chamber. It is likely that sheeted dikes in the fast spreading ridges are emplaced at the apparent LNB between the upper and lower crust.

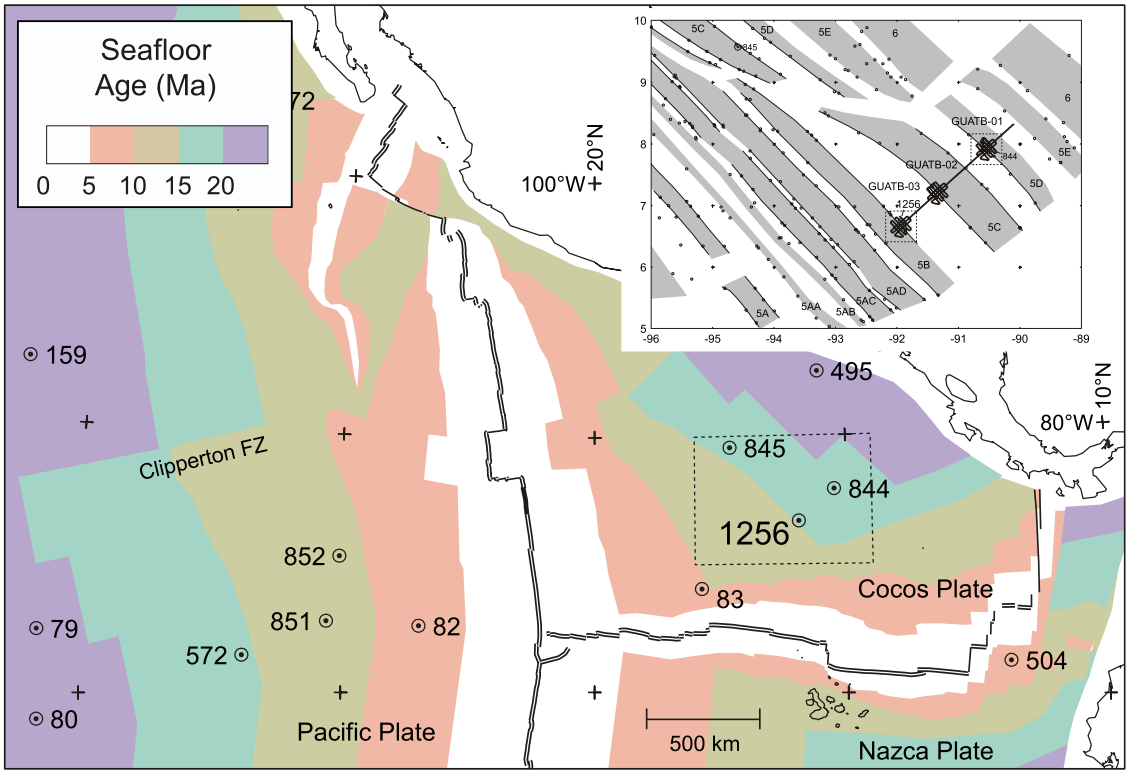

Figure 1. Age map of the Cocos plate and corresponding regions of the Pacific plate after *Teagle et al.* [2006]. Isochrons at 5 Ma intervals have been converted from magnetic anomaly identifications according to the timescale of *Cande and Kent* [1995]. Selected DSDP and ODP sites that reached basement are indicated. FZ, fracture zone. Details of isochrons inferred from magnetic anomalies near Site 1256 (broken square) are shown in the right. Shading shows normal magnetic polarity, based on digitized reversal boundaries (small circles [after *Wilson*, 1996]). Bold line shows location of Guatemala Basin multichannel seismic track lines from the site survey cruise EW9903 conducted in March–April 1999 [*Wilson et al.*, 2003b]. Anomaly ages: 5A = ~12 Ma, 5B = 15 Ma, and 5D = ~17 Ma.

[4] Recent drilling on ODP Leg 206 and IODP-Expeditions 309 and 312 at Site 1256 recovered only a thin interval of sheeted dikes beneath a thicker sequence of extrusive rocks [*Teagle et al.*, 2006; *Wilson et al.*, 2003a, 2006], contrary to the general observations of thin volcanic and thick dike sections in fast spread oceanic crust in Hess Deep [*Francheteau et al.*, 1992; *Hurst et al.*, 1994; *Karson*, 2002; *Karson et al.*, 1992] and in the Oman ophiolite [*Umino et al.*, 2003]. Drilling at Site 1256 in the Guatemala Basin on Cocos plate off Costa Rica, was first initiated on ODP Leg 206. Hole 1256D is drilled into upper oceanic crust formed 15 Ma ago at the EPR during a period of superfast spreading (220 mm/a [*Wilson*, 1996]). Leg 206 penetrated the 250-m thick sediments and then a further 500 m into the basaltic basement (Figures 1 and 2). Subsequent drilling on IODP Expeditions 309 and 312 deepened the hole through a 811-m thick sequence of extrusive rocks, a relatively thin (346 m) sheeted dike complex and eventually reached gabbroic rocks at 1157 m subbasement (msb; 1407 m below seafloor, mbsf). A further ~100 m of gabbroic rocks with subsidiary dike screens were drilled and Hole 1256D currently has a total depth of 1507 mbsf.

[5] The upper crustal structure revealed by deep ocean drilling at Site 1256 provides insight into the shallow magma plumbing and hydrothermal systems beneath fast spreading axes and a good opportunity to test the apparent LNB model for the origin of the sheeted dike complex. This paper documents the extrusive rock-dominated crust formed at a superfast spreading rate at Site 1256. We present a new model for the formation of the sheeted dike complex involving the dynamic balance between the tectonic stresses controlled by plate spreading and varying supplies of magma to the upper crust.

2. Lithostratigraphy of the Upper Oceanic Crust in ODP Hole 1256D

[6] Core descriptions of the 881-m thick sequence of extrusive rocks drilled in Hole 1256D indicate

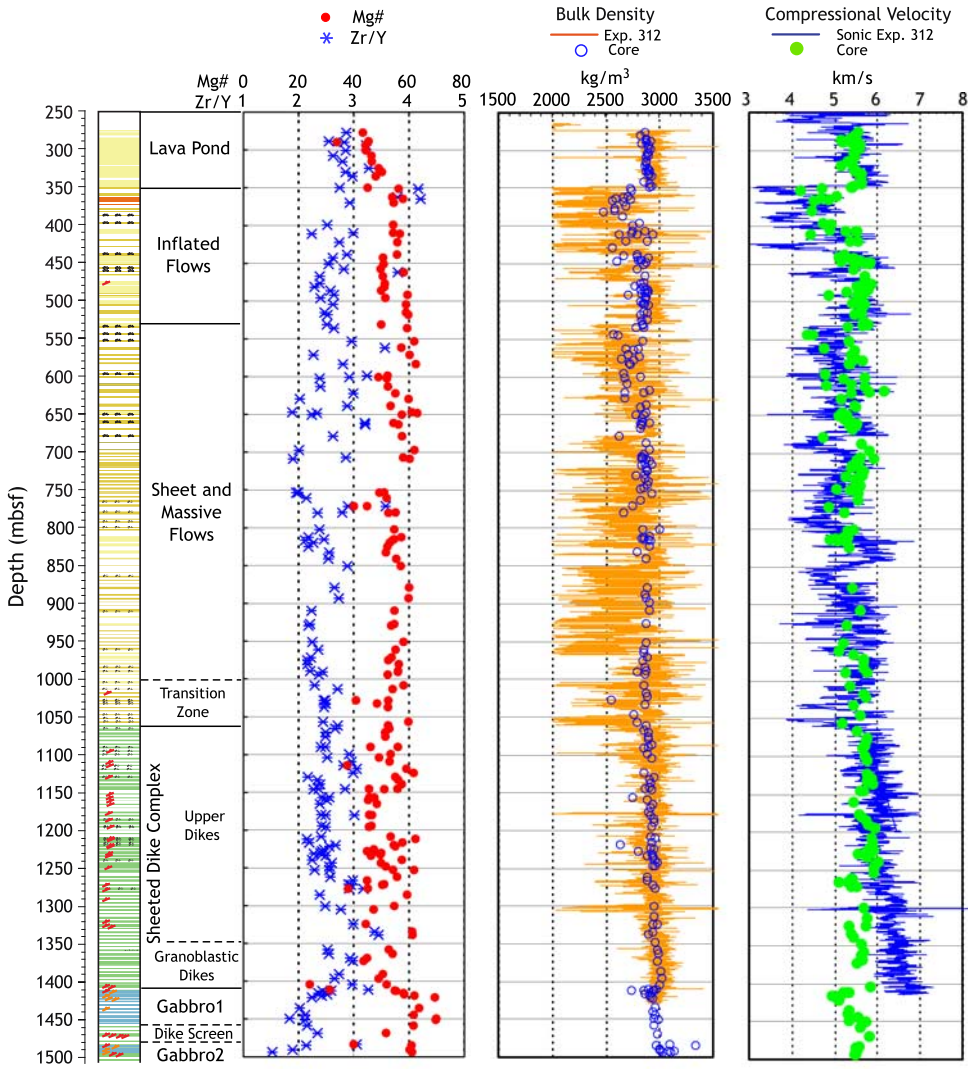

Figure 2. Downhole variations of whole rock Mg# and Zr/Y ratios, lithodensity and bulk densities of core samples, and compressional (P wave) velocities plotted along with lithostratigraphy of ODP Hole 1256D. Whole rock analyses are taken from *Teagle et al.* [2006], and densities and compressional wave velocities determined by the wireline logging and on core samples are available from the IODP core log database: http://iodp.ldeo.columbia.edu/DATA/IODP/index.html.

that sheet flows dominate >96% of the recovered cores (Figure 2), whereas electrical and acoustic imageries suggest that sheet flows comprise ~64% of the extrusive section and approximately 19% and 17% are pillow flows and hyaloclastites, respectively [*Einaudi et al.*, 2005; *Teagle et al.*, 2006; *Tominaga et al.*, 2007; *Wilson et al.*, 2003a, 2006]. The uppermost >74 m of the basement is a thick massive lava unit (Lava Pond) interpreted as a ponded flow accumulated in a fault-bounded basin ~5–10 km off axis [*Wilson et al.*, 2003a; *Crispini et al.*, 2006; *Umino*, 2007]. On the basis of features within the recovered core the lower extrusive sequences are divided into the Inflated Flows (350.3–533.9 m below seafloor: mbsf), presumably emplaced on subhorizontal foot of the rise and the Sheet and Massive Flows (533.9–1004.2 mbsf) that accumulated on the rise slope and crest [*Teagle et al.*, 2006]. The Inflated Flows are typically characterized by the occurrence of subvertical elongate fractures filled with quenched glass and hyaloclastite (e.g., Sections 206-1256D-21R-1 and 40R-1) at the top of the lava flows. On the subhorizontal foot of the southern EPR, these features are observed on inflated subaqueous tumuli associated with lobate sheet flows [*Auzende et al.*, 1996; *Kisimoto and Hilde*, 2004] and are interpreted to indicate flow-lobe inflation that

requires eruption onto a subhorizontal surface, less than a few degrees [*Umino et al.*, 2000, 2002]. The presence of recrystallized flow-lobe margins that were coalesced together (Interval 206-1256D-37R-2, 14–18 cm) are also characteristic to such inflated flow lobes [*Wilson et al.*, 2003a]. This implies that both the Lava Pond and the Inflated Flows formed off axis, suggesting a total thickness of off-axis lavas of 284 m. The electrofacies analysis of wireline logging data has identified a pillow-dominated stratigraphic level between 700 and 800 mbsf in the middle of the Sheet and Massive Flows [*Tominaga et al.*, 2007]. These pillows can be correlated to those on the present East Pacific Rise slope [*Auzende et al.*, 1996; *Kisimoto and Hilde*, 2004]. Therefore, at least the lower half of the Sheet and Massive Flows are considered to have been emplaced on the rise axis.

[7] The lithologic Transition Zone (1004–1061 mbsf) is marked by the first occurrences of subvertical igneous contacts and mineralized breccias. This zone coincides with a stepwise increase in alteration grade with lavas partially altered to low-temperature phases (<150°C; clay minerals, iron oxyhydroxides) giving way to rocks partially altered to chlorite and other greenschist minerals (~250°C or more). Below 1060 mbsf the Sheeted Dikes comprise massive basalt and dolerite with common subvertical chilled margins. The true dip of the chilled margins ranges from 50° to 90° with a mode at ~70°–75°. Oriented electrical and acoustic images indicate that the dike margins dip steeply to the northeast. The sheeted dikes are also characterized by the first notable occurrence of systematic conjugate veins. Many of these dike margins are associated with, or highly disrupted by, diffuse veining and brecciation (Figures 3a and 3b). Thin (<2 cm thick) dikes and chilled margins of some thicker dikes intruded into water-filled cracks were quenched and fragmented into glassy to aphanitic clasts, with associated hydrofracturing and mineralization. Glassy chilled margins are still present at 1210 mbsf, suggesting that host rock temperatures were significantly cool to quench the magmas and hydrothermal mineralogy associated

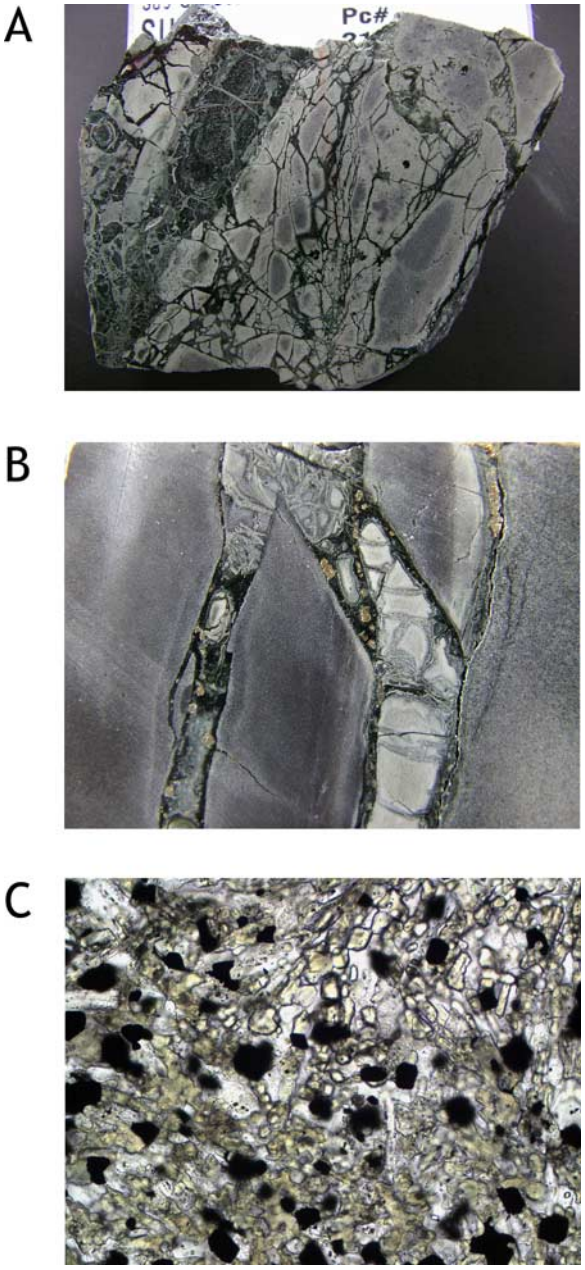

Figure 3. (a and b) Occurrences of fragmental dikes in the Upper Dikes and (c) a microphotograph of metamorphosed dolerite dike in the Granoblastic Dikes. (a) Fragmented dikes suffered from intense hydrothermal alteration along vein networks filling fractures. Note the thin dikelet on the top left in situ fragmented into hyaloclastic materials now replaced by dark green chlorite (Sample 309-1256D-161R-1, 115–119 cm; 1211.35–1211.39 mbsf; field of view (FOV) = 5.5 cm). (b) In situ fragmented dikelet intruded into a thicker dike margin. Note hydrothermal alteration minerals of dark green chlorite and patchy pyrite in vein networks filling the fractures in the dikelet and along the thicker dike margin. (Sample 309-1256D-166R-1, 82–87 cm; 1233.42–1233.38 mbsf; FOV = 3.5 cm) (c) Occurrence and paragenesis of metamorphic clinopyroxene. Isolated single crystals of anhedral granular secondary clinopyroxene in a mineral assemblage of actinolite hornblende, albite-rich plagioclase and magnetite, and a patchy texture. (Thin Section 39, Sample 312-1256D-198R-1, 46–49 cm; 1369.46–1369.72 mbsf; FOV = 0.6 mm; plane polarized light.)

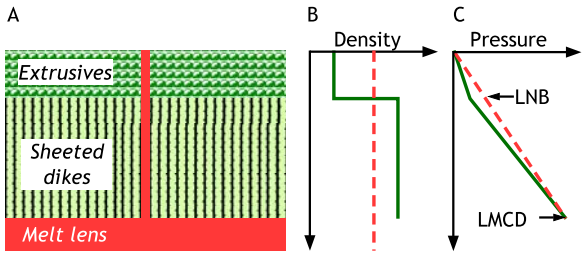

Figure 4. Idealized upper oceanic crust after *Buck et al.* [1997]. (a) The extrusive rocks are expected to be less dense than the magma due to the presence of open cavities between flow lobes and volcaniclastic materials, while the sheeted dikes are considered to be denser than the magma because they are nonvesicular solidified lava. (b) The density profile through the upper crust should be like the green solid lines, while the density of magma is shown by the red broken line. (c) This forms a kink in the lithostatic pressure variation (green solid lines), yielding the level of neutral buoyancy (LNB) at the extrusives–sheeted dikes boundary. Magmastatic pressure at the end of an eruption is given by the red broken line, which crosses the lithostatic pressure curve at the level of magmastatic-lithostatic compensation depth (LMCD).

with dikes indicates crystallization temperatures > 250°C. Common presence of cataclastic and hyaloclastic brecciation of dikes in intimate association with high-temperature (>250°C) mineralization requires that these magmatic-hydrothermal interactions took place beneath or in close proximity to the ridge axis. The lower portion of the sheeted dikes, from 1348–1407 mbsf, are highly altered and locally recrystallized to granoblastic aggregates of clinopyroxene + plagioclase + magnetite + ilmenite ± orthopyroxene (Granoblastic Dikes) (Figure 3c). The plutonic sequence begins at 1407 mbsf, where the lowermost sheeted dikes are intruded by a variety of fine- to coarse-grained gabbros including oxide gabbro, gabbronorite and quartz diorite.

[8] Most extrusives and dikes show moderately evolved (Mg# 40–63) normal mid-ocean ridge basalt (NMORB) compositions in terms of Nb-Zr-Y ratios [*Meschede*, 1986], while the Lava Pond is more strongly differentiated with Mg# 39–50 (Figure 2) [*Wilson et al.*, 2003a, 2006]. Ignoring the Lava Pond which we interpret to have deposited 5–10 km off-axis, the rock density of the extrusive rocks and dikes estimated from wireline logs range from 2001 to 3699 kg/m^3 with an average density of 2757 kg/m^3 (excluding measurements < 2000 kg/m^3, resulting from enlarged borehole diameter > 16 inches; Figure 2). Average *P*-wave velocities (measured on shipboard cubes) of extrusive rocks are 5.36 ± 0.45 km/s in the Inflated Flows and 5.28 ± 1.62 km/s in the Sheet and Massive Flows, whereas the Lava Pond has higher *Vp*s of 5.49 ± 0.21 km/s. Average *Vp* increases through the Transition Zone to 5.70 ± 0.21 km/s in the Sheeted Dikes and is highest in the granoblastic metabasalt dikes. *Vp* in the gabbros is variable around 5.40 ± 0.24 km/s, reflecting strong but variable hydrothermal alteration. FMS-sonic runs show *Vps* generally consistent with the core *Vps* above 1250 mbsf. However, the wireline log *Vp* shows an overall increase up to 6.5 km/s through the sheeted dike complex and apparently deviates from the core *Vps*. Seismic velocity model based on inversion of refraction data shows *Vp* of 4.5–5.3 km/s above ~700 mbsf (Layer 2A), which gradually increases >6.5 km/s down to 1200 mbsf [*Wilson et al.*, 2003a]. The wireline *Vp* is generally consistent with, but is slightly lower than the seismic model *Vp*.

3. Lithostatic Versus Magmastatic Pressure Variations in the Upper Oceanic Crust of Hole 1256D

[9] Normal mid-ocean ridge basalt (NMORB) flows are generally only poorly vesicular with vesicle contents rarely exceeding a few percent except for large subhorizontal blisters beneath the upper crust of sheet flows [*Allan et al.*, 1989; *Sato et al.*, 1978; *Wilson et al.*, 2003a; *Teagle et al.*, 2006]. Ubiquitous quenched glass on the surface of flows with a few vesicles (most probably due to less soluble CO_2 [*Johnson et al.*, 1994]) as well as the undersaturation of water in basaltic magmas at the 2000–2600 m water depths of the summit of mid-ocean ridges indicate that erupting magmas are virtually vesicle free. Under such conditions, it has been suggested that the principal driving force of eruption is buoyancy caused by density contrast between the dense upper crust overlying an axial magma chamber (AMC) filled with less dense magma (Figure 4) [*Buck et al.*, 1997; *Gregg et al.*, 1996]. If the pressure gradient through the conduit is disregarded then an eruption will cease when the magmastatic pressure at the bottom of the magma column within the conduit becomes equal to the lithostatic pressure at the same depth [*Buck et al.*, 1997]. Although vesicle-free magma becomes denser as it cools to solidified lava, the uppermost extrusive section tends to be less dense than the source magmas because there are voids and fractures in between flow lobes, some filled with secondary minerals, as well as intervening

Table 1. Major Element Compositions of Lava Samples From Hole 1256D Used for Magma Density Estimates[a]

	Dense Magma 206-1256D-29R-1, 107–110 cm	Light Magma 206-1256D-63R-1, 81–83 cm
SiO_2	51.36	51.36
TiO_2	1.45	1.04
Al_2O_3	13.79	14.18
FeO*	12.42	9.84
MnO	0.22	0.21
MgO	6.88	8.95
CaO	11.19	11.89
Na_2O	2.46	2.19
K_2O	0.12	0.24
P_2O_5	0.11	0.08

[a] Recalculated on an anhydrous basis. FeO*, total Fe as FeO.

low-density volcaniclastic materials and sediments (Figure 4). In contrast, the sheeted dikes below the extrusive rocks are denser than magmas because they are rarely vesicular and are closely packed with few open interstices [*Alt et al.*, 1993; *Anderson et al.*, 1985; *Becker et al.*, 1988; *Dick et al.*, 1992; *Teagle et al.*, 2006; *Umino et al.*, 2003; *Wilson et al.*, 2003a, 2006]. It follows that the depth at which the load of the magma column compensates for the overburden of the upper crust must be somewhere within the upper crust overlying the AMC and this will be referred to as the lithostatic-magmastatic compensation depth (LMCD), hereafter. The LNB will lie above the LMCD where the excess of magmastatic over lithostatic pressure is largest (Figure 4).

[10] To investigate lithostatic and magmastatic pressure variations in Hole 1256D crust, lithodensity wireline logs and density estimates based on the Hole 1256D lava compositions were used. Lithostatic pressure variation through the upper crust when Hole 1256D is located on the rise axis was estimated by integrating all density data with depth. A few lithodensity measurements <2000 kg/m^3 are too low for the basement compared to the observed core bulk densities (2820 ± 100 to 2860 ± 70 kg/m^3) and these data were eliminated for the lithostatic pressure estimate. Although most eruptions are limited to a narrow volcanic zone on the rise crest in fast spreading mid-ocean ridges, off-axis seamounts erupted within a few kilometers from the rise axis are common along the southern EPR [*White et al.*, 1998]. Considering the width of the AMC beneath the magmatically robust southern EPR (<1.5 km [*Hooft et al.*, 1997]), crustal loads of wider areas than the axial volcanic zone must contribute to the lithostatic pressures which affect dike intrusions from the AMC. Therefore, we integrated all loads below the Lava Pond (>350.3 mbsf) to estimate the lithostatic pressure variation. The uppermost Lava Pond in Hole 1256D was excluded because it is considered to be emplaced ~5–10 km off axis [*Wilson et al.*, 2003a], and would not have contributed to the lithostatic pressure variation at the rise axis. Although the exact locations of the emplacement of the suspected off-axis extrusive rocks remain uncertain, excluding both the Lava Pond and the Inflated Flows from the lithospheric pressure estimates yield a calculated LMCD between 91 and 248 m shallower than the estimates that include the Inflated Flows. However, both these estimates give essentially the same result, and indicate that the LMCD lies at very shallow level in the crust. The depth of the AMC is another unknown factor and probably has migrated upward and downward in relatively short timescale <100,000 years in response to temporal heat balance between the amount of hydrothermal cooling and heating by the supplied magma from below [*Hooft et al.*, 1997]. The sources of the dikes and lavas could have been deeper than the gabbros encountered at 1407 mbsf in Hole 1256D, however, the final conclusions do not change because of the same reason above.

[11] Magma densities were estimated using "adabat_1ph" [*Smith and Asimow*, 2005] run in MELTS [*Ghiorso and Sack*, 1995] mode for two representative magma compositions at liquidus temperatures and at appropriate pressures between the top of the postulated AMC (now frozen as gabbros) assuming the rise axis was at 2600 m water depth. Primitive (MgO 8.95, FeO* 9.84 wt%) and differentiated (MgO 6.88, FeO* 12.42 wt%) end-member compositions were chosen from the lava flows below the Lava Pond, as representative of the range of magma densities (Table 1). Ferric/ferrous ratios of magmas were estimated by the method of *Kress and Carmichael* [1991] assuming oxygen fugacity of 2 $\log_{10}$ units below the quartz-fayalite-magnetite buffer for MORB magmas [*Christie et al.*, 1986].

[12] The downhole lithostatic pressure for the Site 1256 crust increases steadily from 26 MPa (hydrostatic pressure at 2600 m in water depth) on the rise axis to 55 MPa at 1050 m below the seafloor at the top of postulated AMC (Figure 5). The range of densities of magmas at the AMC top is estimated to be 2691 and 2718 kg/m^3. The magma densities are

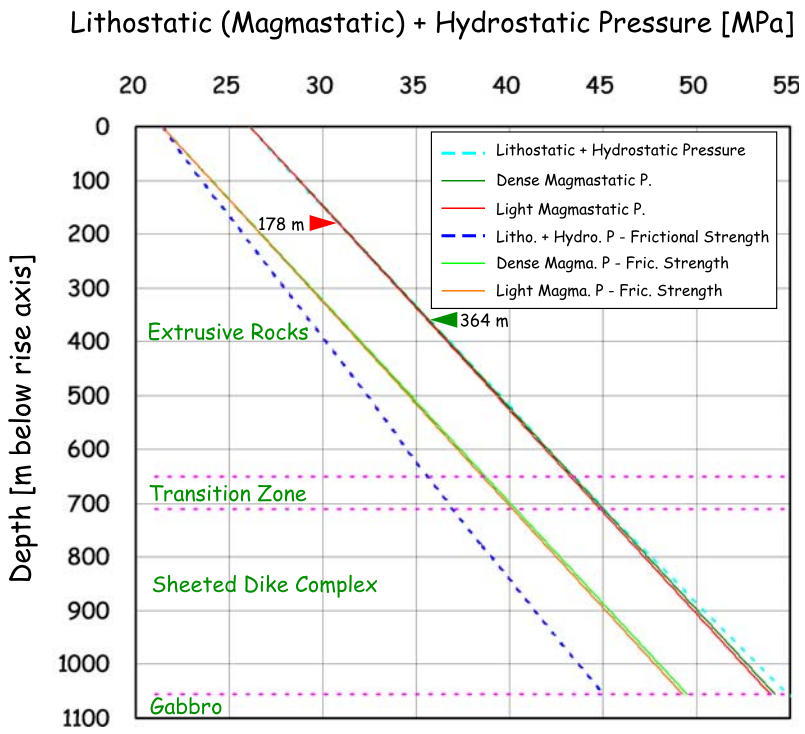

Figure 5. Estimated lithostatic and magmastatic pressure (+hydrostatic pressure) variations in the Hole 1256D crust when it was on the rise axis below 2600 m deep water. The curve of lithostatic pressure (light blue broken curve) crosses those of the dense (green curve) and light (red curve) magmas at 364 m and 178 m below the rise axis, respectively. Blue broken curve shows the minimum limits of the horizontal stress by subtracting the frictional strength of the crust from the lithostatic pressure. The light green and orange curves are magmastatic pressure variations of the dense and light magma columns, respectively. The depths of lithostratigraphic subdivisions are shown by horizontal pink broken lines.

slightly higher than the porous upper extrusives but generally lower than the majority of dense sheet and massive flows and intrusive rocks. Thus, magmastatic pressures are slightly higher than the lithostatic pressure curve only at shallow levels of the crust. However, the magmastatic pressure is lower than the lithostatic pressure in most parts of the crust as the sheet flow-dominated extrusive rocks lose open cavities and fractures, giving way to massive vesicle-free sheeted dikes occurring at depths. Consequently, the magmastatic pressures are lower than the lithostatic pressure in most of the depth range through the upper crust above the AMC. The LMCD is estimated to lie at 178 m and 364 m below the rise axis for light and dense magmas, respectively. Unlike the conceptual model of density profile of the upper oceanic crust described above (Figure 4), the lithostatic pressure curve is almost linear and lacks a kink caused by density contrast between the extrusive rocks and the sheeted dikes. Because of this, the differences between the lithostatic and magmastatic pressures are only minimal above the LMCD. The bulk densities applied for the uppermost extrusive rocks could be too high for those on the ridge axis, which might have increased with change in porosity by precipitation of secondary minerals in open cavities and compaction due to the load of off-axial products on route to the present position. However, total amounts of secondary minerals are minimal through the hole. The estimated density structures beneath the present EPR are generally concordant with the observed density profiles of Hole 1256D except the uppermost 100–200 m with smaller densities <2600 kg/m^3 for the present EPR crust [*Hooft et al.*, 1997]. Incorporating such a thin light carapace will slightly alter the calculated lithostatic pressures but does not affect the conclusions. We think the lithostatic-magmastatic pressure variations of Hole 1256D are the consequences of sheet-flow dominated superfast spread oceanic crust [*Bonatti and Harrison*, 1988; *Meyer and White*, 2007] that is uniformly dense and has no drastic change in bulk density throughout the entire upper crust. This stress condition is similar to that of the conceptual model for dike intrusion cycle in

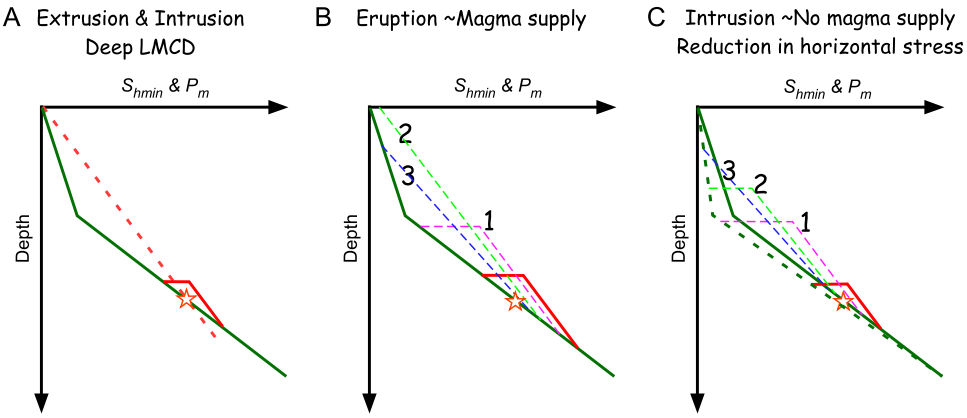

Figure 6. (a) Schematic model for crust with the minimum horizontal stress ($S_{h\min}$, green solid lines) and magmastatic (P_m, red broken line) pressures which cross at moderate depth (star, LMCD), where the AMC is situated. Red solid lines (Figures 6a–6c) represent excess pressure of magma in the AMC. Broken lines in Figures 6b and 6c show the excess pressure of magma in a crack which changes in numerical order (from 1 to 3) as the magma-filled crack ascends toward the seafloor. (b) Supply of a new batch of magma increases magmatic pressure of the AMC, resulting in rupturing of the AMC roof and magma ascent thorough a crack. Eruption takes place when the magma head in the crack (broken green line 2) reaches the surface. The eruption ceases as the excess pressure of magma decreases and magma retreats into the crack that closes from above and bottom to solidify as a dike (blue broken line 3). (c) Dike intrusion without an eruption is favored when it is triggered by the increase in horizontal deviatoric stress (from green solid to broken line) without magma supply. As plate movement steadily increases horizontal deviatoric stress in the brittle upper crust, the excess pressure of the AMC magma increases and eventually exceeds the strength of the AMC roof. As a magma-filled crack grows, magma flows into the crack from the AMC. If the supplied magma is not enough, the magma head in the crack cannot maintain sufficient excess pressure for the crack tip to propagate upward. The magma-filled crack will stop growing before reaching the surface, solidifying as a dike without eruption.

Hawaii proposed by *Rubin* [1990], where high-density sheet-like lava flows are the dominant constituents of the volcanic edifices, too.

4. Discussion

4.1. Compensation Depth of Lithostatic and Magmastatic Pressures: Extrusion or Intrusion?

[13] *Buck et al.* [1997] proposed that the LMCD is the depth of the AMC for fast spreading ridges. However, the AMC depth is more likely controlled by the heat balance between hydrothermal circulation and magma supply [*Hooft et al.*, 1997; *Morton and Sleep*, 1985], and the LMCD gives the minimum depth of the AMC as the root of erupting magma (Figure 6a). When the AMC depth is equal to the LMCD, eruption is only possible if there is a new supply of magma to the AMC (Figure 6b). When the excess magmatic pressure (*Pex*) on top of the AMC exceeds the tensile strength (*Ts*) of the chamber roof, fracturing of the roof will take place and magma will begin to ascend through the crack. As magma-filled crack ascends through the upper crust, *Pex* at the magma head in the crack first increases but gradually decreases as the crack tip approaches the surface. If there is a sufficient amount of magma filling the crack, magma will erupt onto the seafloor. With extrusion of magma, the crack decreases in *Pex* and closes from the bottom. The eruption terminates when the magma head in the crack loses Pex and the bottom of the crack rises to the LMCD. As the remaining magma in the crack cools, drain-back of lava occurs with retreat of the magma head into the fissure vent. Finally, the magma in the crack solidifies as a dike. Without supply of new magma, a dike intrusion can also be triggered by the increase in the horizontal deviatoric stress due to plate movement that contributes the increase in *Pex* to overcome *Ts* (Figure 6c). If there is an insufficient volume of magma, most dikes will be trapped at a level between the surface and the LMCD, where the level of neutral buoyancy resides [*Rubin*, 1990, 1995].

[14] In contrast to the assumptions of the model above, the LMCD in Site 1256D occurs at a shallow level within the extrusive rocks, whereas the estimated top of the AMC is at least 690–880 m deeper below the thick sequence of lavas and thin

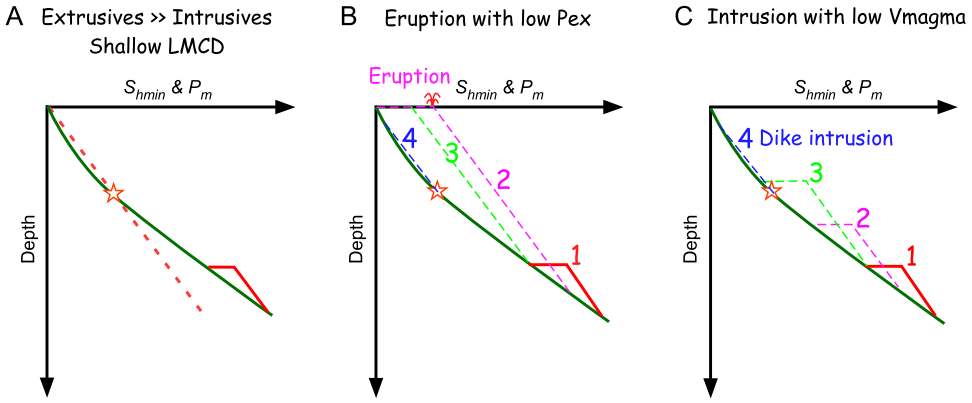

Figure 7. Schematic model for the Hole 1256D crust with a shallow LMCD. Symbols and abbreviations are the same as in Figure 6. (a) AMC lies much deeper than the LMCD, with the excess magmatic pressure as shown by the red solid line. (b) A small increase in excess pressure (shown by red solid line 1) due to supply of a new batch of magma into the AMC causes rupturing of the AMC roof, which leads to ascent of magma through a crack. If there is a sufficient amount of magma, the magma-filled crack grows with an excess pressure as shown by the pink broken line 2, and eventually eruption takes place. As the AMC extrudes magma, it loses the excess magmatic pressure and ultimately shuts off the magma outflow (shown by the green broken line 3). The magma left in the crack continues to extrude, with the crack closing from both above and bottom, which leaves a small amount of magma in the closed crack solidifying as a thin dike (blue broken line 4). (C) In magma-deficient conditions, the AMC loses the excess pressure before the magma-filled crack tip reaches the surface (broken lines 2 and 3). The magma head in the crack cannot maintain sufficient excess pressure to propagate upward until it reaches the surface. As the magma-filled crack moves upward, it closes from bottom and finally stops above the LMCD as a thin dike (broken line 4).

sheeted dike complex. This situation is schematically shown in Figure 7. The AMC is over pressurized and only a small increase in magmatic pressure and/or horizontal deviatoric stress is required to fracture the magma chamber roof (Figure 7b). As magma rises through a crack, *Pex* of the magma head in the crack increases as the crack grows vertically because buoyancy of the magma is proportional to the height of the crack [*Maaløe*, 1987; *Rubin*, 1990, 1995]. As long as the magma head retains a sufficient *Pex* to overcome the rock fracture toughness, the magma-filled crack continues to grow upward and eventually reaches the surface to erupt. As eruption continues, the AMC decreases in *Pex* and ultimately shuts off the magma outflow. As magma in the crack continues to extrude, the crack closes from its lower end, leaving fractured host rocks formed by the intrusion. Quenched magma in the crack against the wall rocks en route will be left as a thin dike (Figure 8). The resulting crack system will provide a locus for fluid circulation with resulting intense alteration and mineralization, and such phenomena are commonly observed throughout the sheeted dikes of Hole 1256D [*Teagle et al.*, 2006]. Reuse of such cracks by a subsequent dike intrusion is very likely, with the consequent underpressure in the reopening cracks ahead of the propagating dike, absorbing pore fluids infiltrating from the host rocks [*Curewitz and Karson*, 1998; *Rubin*, 1995]. Branches of the dike propagating into the fluid-filled cracks will be fragmented into hyaloclastite by contact with hydrothermal fluid. This is the first direct evidence of deep cracking and hydrothermal fluid circulation beneath the ridge axis as suggested by a seismic anisotropy study on the East Pacific Rise at 9°N [*Tong et al.*, 2004]. In the Troodos ophiolite, fracturing caused by episodic diking in the granulite-facies contact aureole within the basal sheeted dikes introduced hydrothermal fluids circulation to deeper levels in the upper crust [*Gillis and Roberts*, 1999].

[15] Magma-deficient conditions will form a dike without extrusion of magma, exhausting all magma in the AMC (Figure 7c). In both magma-sufficient and deficient conditions, the uppermost extrusive section above the LMCD host thin dikes as shallow roots of erupted flows, but these dikes will not evolve to a sheeted dike complex. Because subsequent eruptions bury the dike-hosting section and shift the LMCD upward, the dike-hosting horizons will remain at shallow levels in the crust.

4.2. Conditions of Dike Intrusions and Formation of the Sheeted Dike Complex in Hole 1256D

[16] The lithostatic and magmastatic pressure calculations above suggest that the LMCD at Site

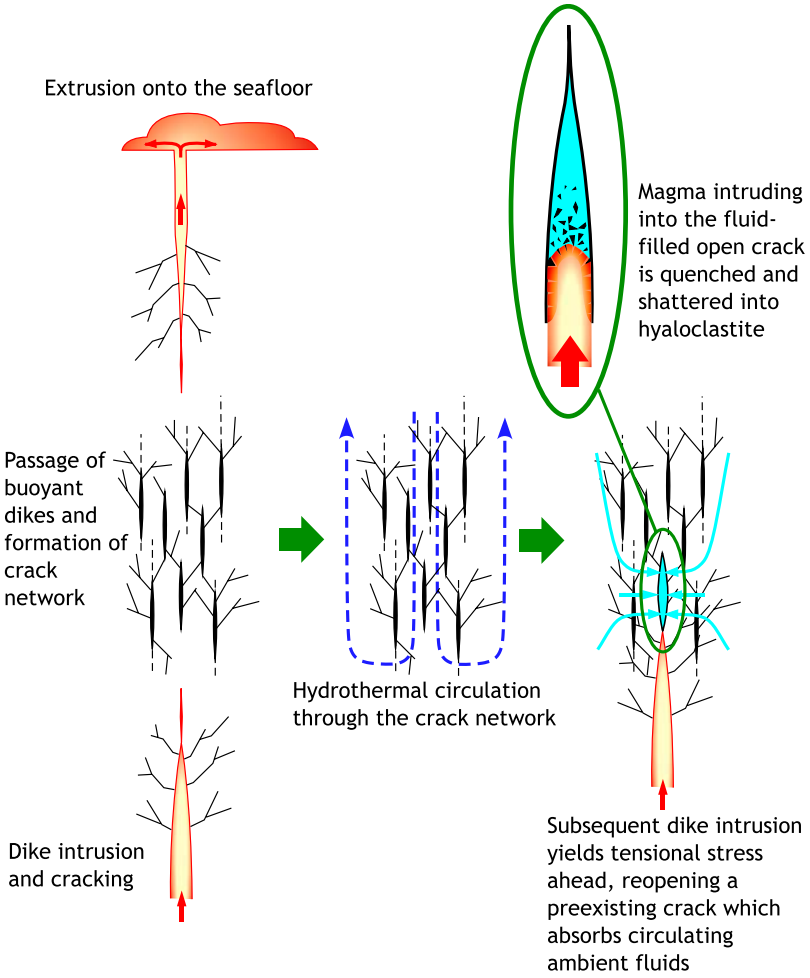

Figure 8. Because of the shallow LMCD, dike intrusion under a small deviatoric stress leads to an eruption which ultimately expels magma out of the crack. As the eruption approaches to the end, the magma-filled crack closes from its lower end, leaving fractured host rocks formed by the intrusion. Such a crack system provides a locus of hydrothermal fluid circulation and localized alteration, as is observed in the crack-dike zone of Hole 1256D. Reuse of such cracks by a subsequent dike intrusion yields an underpressure in opening cracks ahead of the dike, which absorbs pore fluids infiltrating from the host rocks [*Curewitz and Karson*, 1998; *Rubin*, 1995]. Dike propagating into the fluid-filled cracks results in hyaloclastic fragmentation of magma in contact with hydrothermal fluid.

1256 is too shallow to provide an effective LNB to trap ascending dikes in the upper crust. Nevertheless, we have the sheeted dike complex, although the ratio of intrusive to extrusive thickness in Hole 1256D is only 346 m/811 m = 0.43 compared to 1056 m/780.5 m = 1.35 in Hole 504B. The shallow LMCDs and the absence of effective LNB show that density contrast alone cannot explain the formation of the sheeted dike complex. We will consider the genetic conditions of the sheeted dike complex incorporating cooling of magma in the sheeted dikes and dynamics of the stress field at mid-ocean ridges.

[17] Assuming the wall rock temperature of ~200–300°C in the sheeted dike complex as indicated by the hydrothermal mineralogy, rising magma in a crack will solidify to form chilled margins <5 cm thick in 1.5 h [*Carslaw and Jaeger*, 1959], which is comparable to the observed duration of the 1998 eruption at Juan de Fuca Ridge [*Fox et al.*, 2001] and the estimated period of the 1991 April eruption at the northern EPR [*Gregg et al.*, 1996]. Most lava flows observed at the EPR axis are lobate sheets with a typical volume of 0.01–0.1 km^3 with the median value of 0.09 km^3 [*Sinton et al.*, 2002]. Length of fissure vent range from <1 to >18 km and larger eruptions tend to

have been fed through longer fissures [*Sinton et al.*, 2002]. Assuming lava viscosity of 100 Pa·s and fissure lengths and erupted lava volumes of 2–10 km and 0.01–0.1 km^3, respectively, minimum extrusion rates for lobate sheet flows can be estimated as 300–1440 m^3/s using the model of *Gregg and Fink* [1996]. This gives the maximum duration of eruptions of 580–1160 min, during which dike margins will solidify only 10–15 cm in thickness if the wall rock temperature is 300°C [*Carslaw and Jaeger*, 1959]. Consequently, typical eruptions will form dikes with thicknesses less than 30 cm at the end of eruptions. If the extension of the lower part of the upper crust is provided by the emplacement of these dikes, the average eruptive frequency will be every 1.4 years. This is rather higher than the estimate of every 6.9 years for the fast spreading southern EPR [*Sinton et al.*, 2002], even if we take into account the difference in spreading rate between Site 1256 and the present southern EPR. Although it is virtually impossible to know the statistically meaningful frequency distribution of dike thicknesses in a single hole that drilled through only a limited number of dikes, the massive basalt-dolerite structures in the sheeted dike complex indicate the presence of dikes more than a few tens centimeters in thickness [*Teagle et al.*, 2006; *Tominaga et al.*, 2007]. Likewise, the sheeted dike complex in the Oman Ophiolite, considered to have been formed at a fast spreading ridge system, shows a thickness distribution of individual dikes strongly skewed toward thinner dikes, where 36% and 50% of the sheeted dikes are thinner than 20 cm and 40 cm, respectively [*Umino et al.*, 2003]. Conversely, the rest 50% of the sheeted dikes is thicker than 40 cm, ranging in thickness up to 15 m. Thus, the presence of thicker (>30 cm) dikes may also be common in Hole 1256D sheeted dike complex, that urges us to consider the necessary conditions of their formation.

[18] The lithosphere at spreading centers is under a large horizontal tectonic stress due to plate motions that alter the stress gradient through the upper crust to yield an apparent level of neutral buoyancy (apparent LNB) [*Rubin*, 1990, 1995; *Takada*, 1989]. The driving force of dike propagation is the magmatic excess pressure *Pex*, which depends on both the density difference between the magma and the host rock and the gradient of the minimum principal stress [*Takada*, 1989; *Watanabe et al.*, 1999]:

$$Pex = Integral\ of\ \{(D_r - D_m)gdZ - d(S_{h\max} - S_{h\min})/dZ\}$$
$$\text{from } Z_b \text{ to } Z_t$$

where D_r, D_m, g and $S_{h\max} - S_{h\min}$ are the host rock and the magma density, acceleration due to gravity and the horizontal deviatoric stress. Z is the depth and Z_b and Z_t denote the bottom and top depths of the dike. Emplacement of a dike is favored at the apparent LNB because *Pex* is largest there.

[19] The upper limit of the horizontal deviatoric stress is given by brittle rock strength, which is dependent on temperature, strain rate and rock types. In the upper crust below a spreading axis, the horizontal compressive stress is most likely smaller than the vertical stress, because tensile cracks and normal faults are common. Rock deformation is focused on faults, so the rock strength is given by the frictional strength of fault planes rather than by the brittle rock strength [*Sibson*, 2002];

$$F_s = 0.75nS_v(1 - b)$$

where F_s is frictional strength, n is coefficient of internal friction and given as 0.4 for normal faults [*Byerlee*, 1978], S_v is vertical stress and given as D_rgZ, and b is a ratio of fluid pore pressure to vertical stress. As hydrostatic fluid pressure prevails in shallow fluid-saturated crust, we may assume $b = 0.4$ [*Sibson*, 2002]. Then, the frictional strengths at the top and bottom of the upper crust are 4.7–9.9 MPa, which gives the lower limit of the minimum horizontal stress under elastic strain due to the plate spreading (Figure 5).

[20] Because of a large thermal gradient ~50°C/100 m, from greenschist through amphibolite and granulite facies to hypersolidus temperatures in the lowermost sheeted dikes and the roof zone of the AMC [*Gillis and Roberts*, 1999; *Jupp and Schultz*, 2000; *Teagle et al.*, 2006], the rheology of the host rocks largely changes from brittle basalt dikes through viscoelastic dolerite and gabbros to plastic hypersolidus roof zone mushes. As a result, the applied stress tends to concentrate in the brittle upper crust and the reduction in the horizontal stress parallel to the spreading direction becomes larger with depth, attaining the maximum at the bottom of the sheeted dike complex (Figure 9a).

[21] A dike intrusion begins when the excess pressure (*Pex*) overcomes the tensile strength (*Ts*) of the AMC roof. Increase in both horizontal deviatoric stress ($Sv - Sh_{\min}$) and magmatic pressure of the AMC contribute the increase in *Pex*. When the increase in the deviatoric stress surpasses that of magmatic pressure, the dike intrusion is

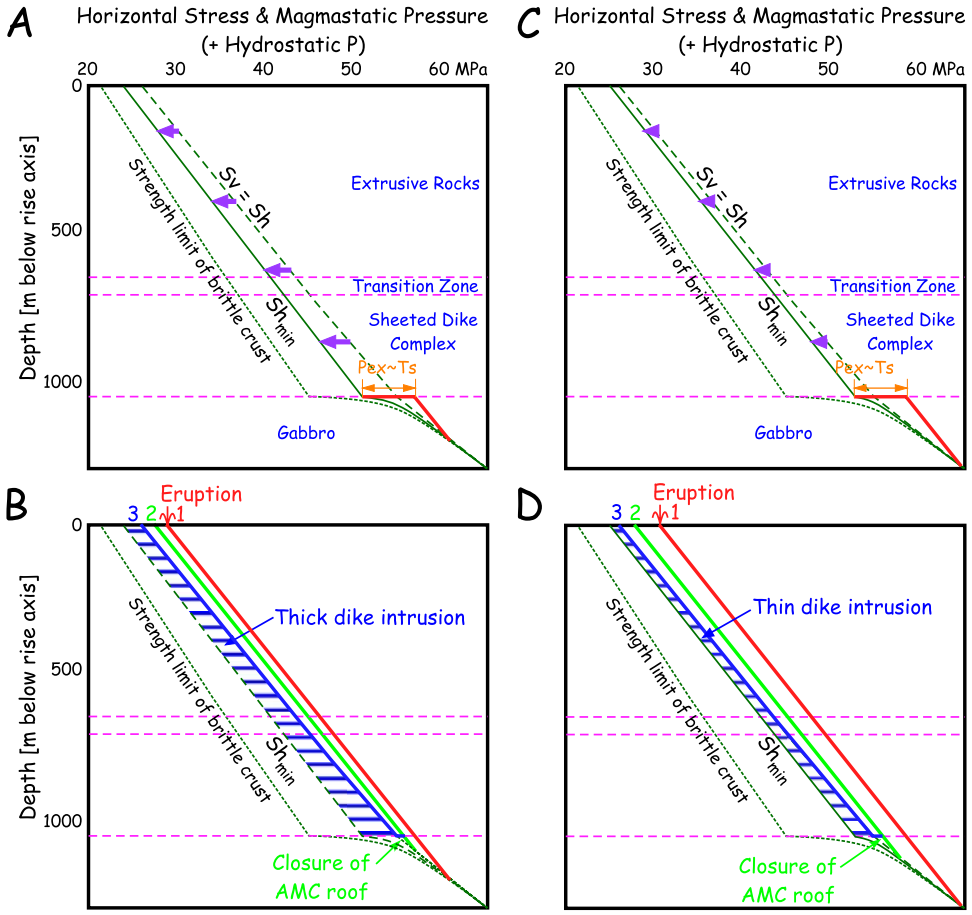

Figure 9. Model of dike emplacement at the apparent level of neutral buoyancy (ALNB) in the upper crust generated under a horizontal deviatoric stress. (a) Green solid curve shows the reduction of horizontal stress (Sh_{min}) normal to the rise axis from "$Sh = Sv$" to "Sh_{min}," caused by elastic and viscous deformation of the brittle upper crust and ductile lower crust in response to plate movement. This generates an ALNB through the upper crust, which can accommodate a thick dike. Reduction in Sh_{min} is largest at the bottom of the sheeted dike complex, and Sh_{min} rapidly increases to the lithostatic pressure through the ductile gabbro-mush zone surrounding the AMC. The increase in *Pex* is mainly caused by the increase in the horizontal deviatoric stress ($Sv - Sh_{min}$). A dike intrusion begins when the excess pressure (*Pex*) overcomes the tensile strength (*Ts*) of the AMC roof. (b) If sufficient magma is available, the head of magma filling the crack reaches the surface to extrude with a large excess pressure (shown by the red line 1). As eruption continues, cooling of magma in the crack and the decrease in *Pex* to a certain level will lead to a closure of the vent of the AMC roof (light green line 2). The magma-filled crack begins to close from the bottom, extruding magma exceeding the amount emplaced as a dike, which relaxes the deviatoric stress in the upper crust. At the end of the eruption, a thick dike is emplaced through the entire upper crust (blue line 3; the horizontally hatched area denotes the amount of stress relaxed by the dike intrusion). (c) In magma-rich conditions, the increase in *Pex* is mainly caused by the increase in the magmatic pressure of the AMC. (d) Eruption occurs with a large absolute magmatic pressure (red line 1) and under a small deviatoric stress. Because the dike intrudes under a small deviatoric stress, the emplaced dike (blue horizontally hatched area) should be thinner than in Figure 9b.

promoted by a large deviatoric stress but with a small absolute magmatic pressure (Figures 9a and 9b). If sufficient magma is available, the head of magma filling the crack reaches the surface to extrude with a large excess pressure. As eruption continues, cooling of magma in the crack and the decrease in *Pex* to a certain level will lead to a closure of the vent of the AMC roof. For a two-dimensional dike with a thickness $2w$ and a height of $2l$, elastic pressure for dike widening ΔP is given by

$$\Delta P = Pm - Sh_{min} = M(w/l)$$

where M is elastic stiffness and is approximately several GPa in nature [*Rubin*, 1995]. Given M to be 5 GPa and $2h$ of 1000 m, the elastic pressure is 1.5–2 MPa if the dike thickness is 30–40 cm. Considering the dike margins solidifying during typical eruptions to be ~15 cm in thickness, $Pex \sim 1$ MPa on the AMC roof would be the critical excess pressure to maintain the magma conduit. In addition to the solidification of dike margins, relaxation of the deviatoric stress by the dike intrusion and the outflow of magma from the AMC reduce $Pex < 1$ MPa and ultimately choke the conduit. The magma-filled crack is detached from the AMC and begins to close from the bottom. Magma in the crack continues to extrude, leaving a thick dike in the upper crust (Figure 9b).

[22] The amount of magma to be emplaced as a dike depends on the accumulated deviatoric stress, the excess magmatic pressure and the volume of available magma. A large deviatoric stress field enables a thick dike intrusion associated with or without an eruption. If sufficient magma is supplied, eruptions will follow dike intrusions (Figure 9b). To the contrary, magma-starved conditions lead only to a dike intrusion without any eruption. All magma in the AMC may be exhausted for a dike emplaced in some part of the upper crust. A magma-filled crack grows as the AMC expels magma into the crack. The crack head continues to rise as far as it retains sufficient *Pex* to overcome the surrounding rock fracture toughness, while the crack bottom closes as the magma-filled crack moves upward. Finally the dike relaxes the deviatoric stress mainly of the lower upper crust where the dike is emplaced. This situation is consistent with the hydrothermal circulation model proposed for the magma-starved ridge segments, where deep magma intrusions and crustal permeability control the vent locations and hydrothermal activity [*Haymon*, 1996].

[23] On the other hand, magmatically robust ridge segments would have high supply rates of magma to the AMC, which gives rise to a rapid increase in magmatic pressure (Figure 9c). This raises the contribution of the AMC pressure to the increase in the excess pressure compared to that of the accumulation of deviatoric stress due to plate movement, which results in a dike intrusion under a small deviatoric stress and a large absolute magmatic pressure (Figure 9d). This condition is relatively compressive compared to that under a large deviatoric stress and allows only a thin dike emplacement in the upper crust. Thus, the supplied magma to the crust is more likely to extrude onto the seafloor. Common presence of AMC reflectors beneath the fast spreading EPR [e.g., *Hooft et al.*, 1997] strongly suggests magma-rich conditions for faster spreading ridge segments, which allows more magma to erupt rather than only to remain in the upper crust as a dike. This explains the high ratio of the extrusive to intrusive rocks in the superfast spread oceanic crust at Site 1256. Because accumulation rate of deviatoric stress depends on the plate movement, it is considered to be more stable than supply rate of magma to AMCs, which may vary on the order of 1,000 to 100,000 years [*Reynolds et al.*, 1992; *Scheirer and Macdonald*, 1993; *Shah et al.*, 2003]. A subtle fluctuation in magma supply rate may change the contribution of the absolute magmatic pressure to the increase in excess pressure, which results in different ratios of magma partitioning into the extrusive and intrusive rocks in the upper crust.

5. Conclusions

[24] ODP Hole 1256D is the first successful drill hole in the 40-year-long history of scientific ocean drilling to successfully penetrate the entire upper oceanic crust formed at the superfast spreading EPR. The 250-m thick sediments are underlain by 811 m of extrusive rocks with minor dikes, underlain by 346 m of subvertical sheeted dikes. Hole 1256D was then deepened a further 105 m into the upper gabbroic rocks. Sheet flows are the dominant flow type with minor intervals of pillow lava and hyaloclastite. An intimate association of brecciation, dike intrusions and hydrothermal mineralization characterizes the transition zone and the sheeted dikes, where brecciated massive basalts is cut by numerous fine veins and cataclastic shear zones, and thin glassy to aphanitic dikes are in situ fragmented into hyaloclastite.

[25] Using lithodensity logging data and magma density calculations, lithostatic and magmastatic pressure variations through the upper crust were estimated for when the Hole 1256D crust was at the rise axis. The dense, sheet flow-dominated crust will have the LMCD at a very shallow level. This is a geometry that favors eruption rather than dike intrusion and density contrast alone (the LNB-control model) cannot explain the formation of the sheeted dike complex. Fractures resulting from the passage of buoyant magmas within dikes were the locus for intense hydrothermal circulation and provided pathways for subsequent dike intrusions.

[26] Considering the period of eruptive episodes, relatively thin (<30 cm) dikes can be formed by cooling and solidification of uprising magma as dike margins before the dike closes at the end of eruption. Thicker (>30 cm) dikes form under a large horizontal deviatoric stress established by consistent plate movement during quiescent periods between each intrusion/extrusion episode. Such a thick dike intrusion may be associated with or without eruption, depending on the amount of magma supplied to the upper crust. Sufficient magma supply will lead to an eruption, while magma-starved conditions end in only dike intrusion. Importantly, magma-rich conditions expected for superfast spreading ridge segments give rise to a rapid increase in magmatic pressure, which results in a dike intrusion under a small deviatoric stress. This results in the emplacement of only a thin region of sheeted dikes in the upper crust and a preference for magma to extrude, explaining the high ratio of the extrusive to intrusive rocks in the Hole 1256D crust.

Acknowledgments

[27] We thank the ODP Leg 206 and IODP Expedition 309/312 Science Parties (R. Anma, A. Belghoul, J. Carlut, D. M. Christie, R. Coggon, C. Cordier, S. R. Durand, F. Einaudi, L. Galli, Y. Gao, J. Geldmacher, L. A. Gilbert, E. Herrero-Bervera, N. W. Hayman, N. Hirano, S. A. Holter, S. Ingle, J. Koepke, C. Laverne, H. L. Lledo Vasquez, J. MacLennan, S. Morgan, N. Neo, S.-H. Park, M. Reichow, T. Sakuyama, T. Sano, C. E. Smith-Duque, B. Scheibner, S. A. Swift, A. A. Tikku, M. Tominaga, E. A. Veloso Espinosa, D. S. Wilson, T. Yamasaki, S. Yamazaki) and all the members of JOIDES Resolution for our epoch-making cruises to Site 1256. This research used samples and data provided by the Integrated Ocean Drilling Program (IODP). IODP is managed by IODP Management International (IODP-MI), Inc. This paper benefited from critical readings and constructive comments by Scott White, Doug Wilson, an anonymous reviewer, and the G-Cubed editor, Vincent Salters. Susumu Umino, Sumio Miyashita, Ryo Anma, Natsuki Neo, Hideo Sakurai, Tetsuya Sakuyama, Takashi Sano, Masako Tominaga, Toru Yamasaki, Shusaku Yamazaki, and Eugenio A. Veloso Espinosa were supported by the Center of Deep Earth Exploration (CDEX) for travel fares. S. Umino was also supported by Monbusho Grant-in-Aid for Research 18540472.

References

Allan, J. F., R. Batiza, M. R. Perfit, D. J. Fornari, and R. O. Sack (1989), Petrology of lavas from the Lamont seamount chain and adjacent East Pacific Rise, 10°N, *J. Petrol.*, *30*, 1245–1298.

Alt, J. C., et al. (1993), *Proc. Ocean Drill. Program Initial Rep.*, vol. 148, 352 pp., Ocean Drill. Program, College Station, Tex.

Anderson, R. N., et al. (1985), *Proc. Ocean Drill. Program Initial Rep.*, vol. 83, 539 pp., Ocean Drill. Program, College Station, Tex.

Auzende, J.-M., et al. (1996), Recent tectonic, magmatic, and hydrothermal activity on the East Pacific Rise between 17°S and 19°S: Submersible observations, *J. Geophys. Res.*, *101*, 17,995–18,010, doi:10.1029/96JB01209.

Becker, K., et al. (1988), *Proc. Ocean Drill. Program Initial Rep.*, vol. 111, 357 pp., Ocean Drill. Program, College Station, Tex.

Bonatti, E., and C. G. A. Harrison (1988), Eruption style of basalt in oceanic spreading ridges and seamounts: Effect of magma temperature and viscosity, *J. Geophys. Res.*, *93*, 2967–2980, doi:10.1029/JB093iB04p02967.

Buck, W. R., S. M. Carbotte, and C. Mutter (1997), Controls on extrusion at mid-ocean ridges, *Geology*, *25*, 935–938, doi:10.1130/0091-7613(1997)025<0935:COEAMO>2.3.CO;2.

Byerlee, J. D. (1978), Friction of rocks, *Pure Appl. Geophys.*, *116*, 615–626, doi:10.1007/BF00876528.

Cande, S. C., and D. V. Kent (1995), Revised calibration of the geomagnetic polarity timescale for the Late Cretaceous and Cenozoic, *J. Geophys. Res.*, *100*, 6093–6095, doi:10.1029/94JB03098.

Carslaw, H. S., and J. C. Jaeger (1959), *Conduction of Heat in Solids*, 2nd ed., 510 pp., Oxford Univ. Press, London.

Christie, D. M., I. S. E. Carmichael, and C. H. Langmuir (1986), Oxidation states of mid-ocean ridge basalt glasses, *Earth Planet. Sci. Lett.*, *79*, 397–411, doi:10.1016/0012-821X(86)90195-0.

Church, W. R., and R. K. Stevens (1971), Early Paleozoic ophiolite complexes of the Newfoundland Appalachians as mantle-ocean crust sequences, *J. Geophys. Res.*, *76*, 1460–1466, doi:10.1029/JB076i005p01460.

Crispini, L., P. Tartarotti, and S. Umino (2006), Microstructural features of a subaqueous lava from basaltic crust off the East Pacific Rise (ODP Site 1256, Cocos Plate), *Ofioliti*, *31*, 117–127.

Curewitz, D., and J. A. Karson (1998), Geological consequences of dike intrusion at mid-ocean ridge spreading centers, in *Faulting and Magmatism at Mid-Ocean Ridges*, *Geophys. Monogr. Ser.*, vol. 106, edited by W. R. Buck et al., pp. 117–136, AGU, Washington, D. C.

Dick, H. J. B., et al. (1992), *Proc. Ocean Drill. Program Initial Rep.*, vol. 140, 408 pp., Ocean Drill. Program, College Station, Tex.

Einaudi, F., P. A. Pezard, C. Laverne, P. Tartarotti, and L. Crispini (2005), Volcanic structure of fast spreading oceanic crust from borehole geophysics in ODP Hole 1256D, eastern equatorial Pacific, *Geophys. Res. Abstr.*, *7*, Abstract 07220, SRef-ID:1607-7962/gra/EGU05-A-07220.

Fox, C. G., W. W. Chadwick Jr., and R. W. Embley (2001), Direct observation of a submarine volcanic eruption from a sea-floor instrument caught in a lava flow, *Nature*, *412*, 727–729, doi:10.1038/35089066.

Francheteau, J., R. Armijo, J. L. Cheminee, R. Hekinian, P. Lonsdale, and N. Blum (1992), Dyke complex of the East Pacific Rise exposed in the walls of Hess Deep and the structure of the upper oceanic crust, *Earth Planet. Sci. Lett.*, *111*, 109–121, doi:10.1016/0012-821X(92)90173-S.

Gass, I. G., , S. J. Lippard, and A. W. Shelton (Eds.) (1981), *Ophiolite and Oceanic Lithosphere*, Geol. Soc. Spec. Publ., vol. 13, 413 pp., Geol. Soc. London, London.

Ghiorso, M. S., and R. O. Sack (1995), Chemical mass transfer in magmatic processes IV. A revised and internally consistent thermodynamic model for the interpolation and extra-

polation of liquid-solid equilibria in magmatic systems at elevated temperatures and pressures, *Contrib. Mineral. Petrol.*, *119*, 197–212, doi:10.1007/BF00307281.

Gillis, K. M., and M. D. Roberts (1999), Cracking at the magma-hydrothermal transition: Evidence from the Troodos Ophiolite, Cyprus, *Earth Planet. Sci. Lett.*, *169*, 227–244, doi:10.1016/S0012-821X(99)00087-4.

Glennie, K. W., M. G. A. Boeuf, M. W. Hughes Clarke, M. Moody-Stuart, W. F. H. Pilaar, and B. M. Reinhardt (1974), Geology of the Oman Mountains, *K. Ned. Geol. Mijnboukd. Genoot. Verh.*, *31*, 43 pp.

Gregg, T. K. P., and J. H. Fink (1996), Quantification of extraterrestrial lava flow effusion rates through laboratory simulations, *J. Geophys. Res.*, *101*, 16,891–16,900, doi:10.1029/96JE01254.

Gregg, T. K. P., D. J. Fornari, M. R. Perfit, R. M. Haymon, and J. H. Fink (1996), Rapid emplacement of a mid-ocean ridge lava flow on the East Pacific Rise at 9°46′–51′N, *Earth Planet. Sci. Lett.*, *144*, E1–E7, doi:10.1016/S0012-821X(96)00179-3.

Gudmundsson, A. (1988), Effect of tensile stress concentration around magma chambers on intrusion and extrusion frequencies, *J. Volcanol. Geotherm. Res.*, *35*, 179–194, doi:10.1016/0377-0273(88)90015-7.

Gudmundsson, A. (1990), Dyke emplacement at divergent plate boundaries, in *Mafic Dykes and Emplacement Mechanisms*, edited by A. J. Parker, P. C. Rickwood, and D. H. Tucker, pp. 47–62, A. A. Balkema, Rotterdam, Netherlands.

Haymon, R. M. (1996), The response of ridge-crest hydrothermal systems to segmented, episodic magma supply, in *Tectonic, Magmatic, Hydrothermal and Biological Segmentation of Mid-Ocean Ridges*, edited by C. J. MacLeod, P. A. Tyler, and C. L. Walker, *Geol. Soc. Spec. Publ.*, *118*, 157–168.

Hooft, E. E. E., R. S. Detrick, and G. M. Kent (1997), Seismic structure and indicators of magma budget along the southern East Pacific Rise, *J. Geophys. Res.*, *102*, 27,319–27,340, doi:10.1029/97JB02349.

Hurst, S. D., J. A. Karson, and K. L. Verosub (1994), Paleomagnetic study of tilted diabase dikes in fast-spread oceanic crust exposed at Hess Deep, *Tectonics*, *13*, 789–802, doi:10.1029/94TC00845.

Johnson, M. C., A. T. Anderson Jr., and M. J. Rutherford (1994), Pre-eruptive volatile contents of magmas, in *Volatiles in Magmas*, *Rev. Mineral.*, vol. 30, edited by M. R. Carroll and J. R. Holloway, pp. 281–330, Mineral. Soc. of Am., Washington, D. C.

Jupp, T., and A. Schultz (2000), A thermodynamic explanation for black smoker temperatures, *Nature*, *403*, 880–883, doi:10.1038/35002552.

Karson, J. A. (2002), Geological structure of the uppermost oceanic crust created at fast- to intermediate-rate spreading centers, *Annu. Rev. Earth Planet. Sci.*, *30*, 347–384, doi:10.1146/annurev.earth.30.091201.141132.

Karson, J. A., S. D. Hurst, and P. Lonsdale (1992), Tectonic rotations of dikes in fast-spread oceanic crust exposed near Hess Deep, *Geology*, *20*, 685–688, doi:10.1130/0091-7613(1992)020<0685:TRODIF>2.3.CO;2.

Kidd, R. G. W., and J. R. Cann (1974), Chilling statistics indicate an ocean-floor spreading origin for the Troodos complex, Cyprus, *Earth Planet. Sci. Lett.*, *24*, 151–155, doi:10.1016/0012-821X(74)90020-X.

Kisimoto, K., and T. W. Hilde (2004), SHINKAI 6500 observations of the volcanic-tectonic relationships on the SEPR rise crest and western slope at 14°10′S to 14°13′S, *Eos Trans. AGU*, *85*(47), Fall Meet. Suppl, Abstract V53A-0613.

Kress, V. C., and I. S. E. Carmichael (1991), The compressibility of silicate liquids containing Fe_2O_3 and the effect of composition, temperature, oxygen fugacity and pressure on their redox states, *Contrib. Mineral. Petrol.*, *108*, 82–92, doi:10.1007/BF00307328.

Maaløe, S. (1987), The generation and shape of feeder dykes from mantle source, *Contrib. Mineral. Petrol.*, *96*, 47–55, doi:10.1007/BF00375524.

Meschede, M. (1986), A method of discriminating between different types of mid-oceanic ridge basalts and continental tholeiites with the Nb-Zr-Y diagram, *Chem. Geol.*, *56*, 207–218, doi:10.1016/0009-2541(86)90004-5.

Meyer, J. D., and S. M. White (2007), Lava morphology mapping by expert system classification of high-resolution sidescan imagery from the East Pacific Rise, 9°–10°N, *Mar. Geophys. Res.*, *28*, 81–93, doi:10.1007/s11001-007-9015-8.

Moores, E. M., and F. J. Vine (1971), The Troodos massif, Cyprus, and other ophiolites as oceanic crust: Evidence and implications, *Philos. Trans. R. Soc. London, Ser. A*, *268*, 443–466, doi:10.1098/rsta.1971.0006.

Morton, J. L., and N. H. Sleep (1985), A mid-ocean ridge thermal model: Constraints on the volume of axial hydrothermal heat flux, *J. Geophys. Res.*, *90*, 11,345–11,353, doi:10.1029/JB090iB13p11345.

Reynolds, J. R., C. H. Langmuir, J. F. Bender, K. A. Kastens, and W. B. F. Ryan (1992), Spatial and temporal variability in the geochemistry of basalts from the East Pacific Rise, *Nature*, *359*, 493–499, doi:10.1038/359493a0.

Rubin, A. M. (1990), A comparison of rift-zone tectonics in Iceland and Hawaii, *Bull. Volcanol.*, *52*, 302–319, doi:10.1007/BF00304101.

Rubin, A. M. (1995), Propagation of magma-filled cracks, *Annu. Rev. Earth Planet. Sci.*, *23*, 287–336, doi:10.1146/annurev.ea.23.050195.001443.

Ryan, M. P. (1994), Neutral-buoyancy controlled magma transport and storage in mid-ocean ridge magma reservoirs and their sheeted dike complex: A summary of basic relationships, in *Magmatic Systems*, edited by M. P. Ryan, pp. 97–138, Academic, San Diego, Calif.

Sato, H., K. Aoki, K. Okamoto, and B. Fujita (1978), Petrology and chemistry of basaltic rocks from Hole 396B, IPOD/DSDP Leg 46, *Initial Rep. Deep Sea Drill. Proj.*, *46*, 115–141.

Scheirer, D. S., and K. C. Macdonald (1993), Variation in cross-sectional area of the axial ridge along the East Pacific Rise: Evidence for the magmatic budget of a fast spreading center, *J. Geophys. Res.*, *98*, 7871–7885, doi:10.1029/93JB00015.

Shah, A. K., M.-H. Cormier, W. B. F. Ryan, W. Jin, J. M. Sinton, E. Bergmanis, J. Carlut, A. Bradley, and D. Yoeger (2003), Episodic dike swarms inferred from near-bottom magnetic anomaly maps at the southern East Pacific Rise, *J. Geophys. Res.*, *108*(B2), 2097, doi:10.1029/2001JB000564.

Sibson, R. H. (2002), Geology of the crustal earthquake source, in *International Handbook of Earthquake and Engineering Seismology*, vol. 81A, edited by W. H. K. Lee et al., pp. 455–473, Academic, Boston, Mass.

Sinton, J. M., E. Bergmanis, K. Rubin, R. Batiza, T. K. P. Gregg, K. Grönvold, K. C. Macdonald, and S. M. White (2002), Volcanic eruptions on mid-ocean ridges: New evidence from the superfast spreading East Pacific Rise, 17°–19°S, *J. Geophys. Res.*, *107*(B6), 2115, doi:10.1029/2000JB000090.

Smith, P. M., and P. D. Asimow (2005), Adiabat_1ph: A new public front-end to the MELTS, pMELTS, and pHMELTS

models, *Geochem. Geophys. Geosyst.*, *6*, Q02004, doi:10.1029/2004GC000816.

Sturt, B. A., and A. Thon (1978), An ophiolite complex of probably early Caledonian age discovered on Karmoy, *Nature*, *275*, 538–539, doi:10.1038/275538a0.

Takada, A. (1989), Magma transport and reservoir formation by a system of propagating cracks, *Bull. Volcanol.*, *52*, 118–126, doi:10.1007/BF00301551.

Teagle, D. A. H., J. C. Alt, S. Umino, S. Miyashita, N. R. Banerjee, D. S. Wilson, and the Expedition 309/312 Scientists (2006), *Proceedings of the Integrated Ocean Drilling Program*, vol. 309/312, Integrated Ocean Drill. Program Manage. Int. Inc., Washington, D. C., doi:10.2204/iodp.proc.309312.101.2006.

Tominaga, M., S. Umino, J. C. Alt, and D. A. H. Teagle (2007), Determination of volcanostratigraphy at ODP/IODP Hole 1256D — Qualitative and quantitative core-log integration, *Eos Trans. AGU*, *88*(52), Fall Meet. Suppl., Abstract OS51A-0178.

Tong, C. H., R. S. White, M. R. Warner, and the ARAD Working Group (2004), Effects of tectonism and magmatism on crack structure in oceanic crust: A seismic study, *Geology*, *32*, 25–28, doi:10.1130/G19962.1.

Umino, S. (2007), Data report: Textural variation of Units 1256C-18 and 1256D-1 lava pond, with special reference to recrystallization of the base of Unit 1256C-18, *Proc. Ocean Drill. Program Sci. Results*, *206*, 32 pp., Ocean Drill. Program, College Station, Tex., doi:10.2973/odp.proc.sr.206.007.2007.

Umino, S., P. W. Lipman, and S. Obata (2000), Subaqueous lava flow lobes, observed on ROV *KAIKO* dives off Hawaii, *Geology*, *28*, 503–506, doi:10.1130/0091-7613(2000)28<503:SLFLOO>2.0.CO;2.

Umino, S., S. Obata, P. W. Lipman, J. R. Smith, T. Shibata, J. Naka, and F. Trusdell (2002), Emplacement and inflation structures of submarine and subaerial Pahoehoe lavas from Hawaii, in *Hawaiian Volcanoes: Deep Underwater Perspectives*, *Geophys. Monogr. Ser.*, vol. 128, edited by E. Takahashi et al., pp. 85–101, Washington, D. C.

Umino, S., S. Miyashita, F. Hotta, and Y. Adachi (2003), Along-strike variation of the sheeted dike complex in the Oman Ophiolite: Insights into subaxial ridge segment structures and the magma plumbing system, *Geochem. Geophys. Geosyst.*, *4*(9), 8618, doi:10.1029/2001GC000233.

Watanabe, T., T. Koyaguchi, and T. Seno (1999), Tectonic stress controls on ascent and emplacement of magmas, *J. Volcanol. Geotherm. Res.*, *91*, 65–78, doi:10.1016/S0377-0273(99)00054-2.

White, S. W., K. C. Macdonald, D. S. Scheirer, and M.-H. Cormier (1998), Distribution of isolated volcanoes on the flanks of the East Pacific Rise, 15.3°S–20°S, *J. Geophys. Res.*, *103*, 30,371–30,384, doi:10.1029/98JB02791.

Wilson, D. S. (1996), Fastest known spreading on the Miocene Cocos-Pacific plate boundary, *Geophys. Res. Lett.*, *23*, 3003–3006, doi:10.1029/96GL02893.

Wilson, D. S., et al. (2003a), *Proc. Ocean Drill. Program Initial Rep.* [online], vol. 206, Ocean Drill. Program, College Station, Tex. (Available at http://www-odp.tamu.edu/publications/206_IR/206ir.htm)

Wilson, D. S., E. Hallenborg, A. J. Harding, and G. M. Kent (2003b), Data report: Site survey results from cruise EW9903, *Proc. Ocean Drill. Program Initial Rep.* [CD-ROM], *206*, 49 pp. (Available at http://www-odp.tamu.edu/publications/206_IR/chap_04/chap_04.htm)

Wilson, D. S., et al. (2006), Drilling to gabbro in intact ocean crust, *Science*, *312*, 1016–1020, doi:10.1126/science.1126090.